

# A Scaler-Based Data Acquisition System for Measuring Parity Violation Asymmetry in Deep Inelastic Scattering

R. Subedi<sup>a,1</sup>, D. Wang<sup>a</sup>, K. Pan<sup>b</sup>, X. Deng<sup>a</sup>, R. Michaels<sup>c</sup>,  
P. E. Reimer<sup>d</sup>, A. Shahinyan<sup>e</sup>, B. Wojtsekhowski<sup>c</sup>, X. Zheng<sup>a,\*</sup>

<sup>a</sup>University of Virginia, Charlottesville, VA 22904, USA

<sup>b</sup>Massachusetts Institute of Technology, Cambridge, MA 02139, USA

<sup>c</sup>Thomas Jefferson National Accelerator Facility, Newport News, VA 23606, USA

<sup>d</sup>Physics Division, Argonne National Laboratory, Argonne, IL 60439, USA

<sup>e</sup>Yerevan Physics Institute, Yerevan, Armenia

---

## Abstract

An experiment that measured the parity violating asymmetries in deep inelastic scattering was completed at the Thomas Jefferson National Accelerator Facility in experimental Hall A. From these asymmetries, a combination of the quark weak axial charge could be extracted. To achieve this, asymmetries at the  $10^{-4}$  level needed to be measured at event rates up to 500 kHz and the high pion background typical to deep inelastic scattering experiments needed to be rejected efficiently. A specialized data acquisition (DAQ) system with intrinsic particle identification (PID) was successfully developed and used: The pion contamination in the electron samples was controlled at the order of  $2 \times 10^{-3}$  or below with an electron efficiency of higher than 91% throughout the experiment; the systematic uncertainty in the measured asymmetry due to DAQ deadtime was below 0.2%; and the statistical quality of the asymmetry measurement agreed with the Gaussian distribution to over five orders of magnitudes. The DAQ system is presented here with an emphasis on its design scheme, the achieved PID performance, deadtime effect and the capability of measuring small asymmetries.

*Key words:* Jefferson Lab; Hall A; PVDIS; DAQ

*PACS:* 11.30.Er, 12.15.Mm, 13.60.Hb 14.60.Cd 14.65.Bt 29.30.Aj 29.85.Ca

---

<sup>1</sup> Present address: George Washington University, 725 21<sup>st</sup> St, NW, Washington, DC 20052, USA

\* Corresponding author. E-mail: xiaochao@jlab.org; Telephone: 001-434-243-4032; Fax: 001-434-924-4576

28 **1 Introduction**

29 The Parity Violating Deep Inelastic Scattering (PVDIS) experiment E08-011 was  
 30 completed in December 2009 at the Thomas Jefferson National Accelerator Facil-  
 31 ity (JLab). The goal of this experiment [1–3] was to measure with high precision  
 32 the parity violating asymmetry in deep inelastic scattering of a polarized 6 GeV  
 33 electron beam on an unpolarized liquid deuterium target. This asymmetry is sensi-  
 34 tive to the quark weak axial charge  $C_{2q}$  which corresponds to a helicity dependence  
 35 in the quark coupling with the  $Z^0$  boson.

36 For electron inclusive scattering from an unpolarized target, the electromagnetic  
 37 interaction is parity conserving and is insensitive to the spin flip of the incom-  
 38 ing electron beam. Only the weak interaction violates parity and causes a differ-  
 39 ence between the right- and the left-handed electron scattering cross-sections  $\sigma_R$   
 40 and  $\sigma_L$ . The dominant contribution to the parity violation asymmetry,  $A_{PV} \equiv$   
 41  $(\sigma_R - \sigma_L)/(\sigma_R + \sigma_L)$ , arises from the interference between electromagnetic and  
 42 weak interactions and is proportional to the four momentum transfer squared  $Q^2$   
 43 for  $Q^2 \ll M_Z^2$ . The magnitude of the asymmetry is in the order of  $10^{-4}$  or  $10^2$  parts  
 44 per million (ppm) at  $Q^2 = 1$  (GeV/c) $^2$ .

45 The PVDIS asymmetry from a deuterium target is

$$A_{PV} = \left( -\frac{G_F Q^2}{4\sqrt{2}\pi\alpha} \right) \left( 2g_A^e Y_1 \frac{F_1^{\gamma Z}}{F_1^\gamma} + g_V^e Y_3 \frac{F_3^{\gamma Z}}{F_1^\gamma} \right), \quad (1)$$

46 where  $Q^2$  is the negative of the four-momentum transfer squared,  $G_F$  is the Fermi  
 47 weak coupling constant,  $\alpha$  is the fine structure constant,  $Y_1$  and  $Y_3$  are kinematic  
 48 factors,  $x$  is the Bjorken scaling variable, and  $F_{1,3}^{\gamma(Z)}$  are deuteron structure functions  
 49 that can be evaluated from the parton distribution functions and the quark- $Z^0$  vector  
 50 and axial couplings  $g_{V,A}^q$ . From this asymmetry one can extract the quark weak  
 51 vector and axial charges  $C_{1,2q}$ , where the quark weak vector charge is defined as  
 52  $C_{1q} \equiv 2g_A^e g_V^q$  and the quark weak axial charge is given by  $C_{2q} \equiv 2g_V^e g_A^q$  with  $q =$   
 53  $u, d$  indicating an up or a down quark,  $g_{A(V)}^e$  is the electron axial (vector) coupling  
 54 and  $g_{V(A)}^q$  is the quark vector (axial) coupling to the  $Z^0$  boson. In the tree-level  
 55 Standard Model, the  $C_{1,2q}$  are related to the weak mixing angle  $\theta_W$ :  $C_{1u} = -\frac{1}{2} +$   
 56  $\frac{3}{4} \sin^2 \theta_W$ ,  $C_{2u} = -\frac{1}{2} + 2 \sin^2 \theta_W$ ,  $C_{1d} = \frac{1}{2} - \frac{2}{3} \sin^2 \theta_W$ , and  $C_{2d} = \frac{1}{2} - 2 \sin^2 \theta_W$ .  
 57 Although the weak mixing angle and the quark weak vector charge  $C_{1q}$  have been  
 58 measured from various processes [4], the current knowledge on the quark weak  
 59 axial charge  $C_{2q}$  is poor and their deviations from the Standard Model value would  
 60 reveal possible New Physics in the quark axial couplings that could not be accessed  
 61 from other Standard Model parameters.

62 The goal of JLab E08-011 was to measure the PVDIS asymmetries to statistical

63 precisions of 3% and 4% at  $Q^2 = 1.1$  and  $1.9$  (GeV/c)<sup>2</sup>, respectively, and under the  
 64 assumption that hadronic physics corrections are small, to extract the quark axial  
 65 weak charge combination ( $2C_{2u} - C_{2d}$ ). In addition, the systematic uncertainty  
 66 goal was less than 3%. For this experiment, the expected asymmetries were 91 and  
 67 160 ppm respectively at the two  $Q^2$  values. To achieve the required precision, an  
 68 event rate capability of up to 500 kHz was needed.

69 The main challenge of deep inelastic scattering experiments is the separation of  
 70 scattered electrons from the pion background in the spectrometer and detector sys-  
 71 tem. The neutral pions would decay into  $e^+e^-$  pairs, from which the electrons pro-  
 72 duced cannot be rejected by detectors and their effect on the measured asymmetry  
 73 was analyzed in Ref. [3]. Charged pions are produced primarily from nucleon res-  
 74 onance decays and could carry a parity violation asymmetry corresponding to the  
 75  $Q^2$  at which the resonances are produced, typically a fraction of the asymmetry of  
 76 electrons with the same scattered momentum. Assuming a fraction  $f$  of the detected  
 77 events are  $\pi^-$  and  $1 - f$  are electrons, the measured asymmetry is

$$A_m = fA_\pi + (1 - f)A_e, \quad (2)$$

78 where  $A_e$  is the desired electron scattering asymmetry and  $A_\pi$  is the asymmetry of  
 79 the pion background. To extract  $A_e$  to a high precision, one needs to either minimize  
 80 the pion contamination  $f$  to a negligible level, or to correct the measured asymme-  
 81 try for the asymmetry of pions, which itself needs to be measured precisely. For the  
 82 PVDIS experiment, the goal was to control  $f$  to the  $10^{-3}$  level.

83 The experiment used a  $100 \mu\text{A}$  electron beam with a polarization of approximately  
 84 90% and a 20-cm long liquid deuterium target. The two High Resolution Spec-  
 85 trometers (HRS) [5] were used to detect scattered events. While the standard HRS  
 86 detector package and data acquisition (DAQ) system routinely provide a  $10^4$  pion  
 87 rejection with approximately 99% electron efficiency, they are based on full record-  
 88 ing of the detector signals and are limited to event rates up to 4 kHz [5]. This is not  
 89 sufficient for the high rates expected for the experiment. (The HRS DAQ will be  
 90 referred to as “standard DAQ” hereafter.)

91 Recent parity violation electron scattering experiments, such as SAMPLE [6] at  
 92 MIT-Bates, HAPPEX [7–11], and PREX [12] at JLab, focused on elastic scatter-  
 93 ing from nuclear or nucleon targets that are typically not contaminated by in-  
 94 elastic backgrounds. Signals from the detectors can be integrated and a helicity  
 95 dependence in the integrated signal can be used to extract the physics asymme-  
 96 try. An integrating DAQ was also used at the preceding PVDIS measurement at  
 97 SLAC [13,14] in which approximately 2% of the integrated signal was attributed  
 98 to pions. In the Mainz PVA4 experiment [15–17], particles were detected in a total  
 99 absorption calorimeter and the integrated energy spectrum was recorded. Charged  
 100 pions and other background were separated from electrons in the offline analysis  
 101 of the energy spectrum, and the pion rejection is in the order of 100:1 based on the

102 characteristics of the calorimeter.

103 High performance particle identification can usually be realized in a counting-based  
104 DAQ where each event is evaluated individually. In the G0 experiment [18–22]  
105 at JLab, a superconducting spectrometer with a  $2\pi$  azimuthal angle coverage was  
106 used to detect elastically scattered protons at the forward angle and elastic elec-  
107 trons at the backward angle. At the forward angle, protons were identified using  
108 time-of-flight. At the backward angle, pions were rejected from electrons using an  
109 aerogel Cherenkov counter and a pion rejection factor of 125 : 1 or better was re-  
110 ported [22]. The deadtime correction of the counting system was at the order of a  
111 few percent [21,22].

112 While the PVDIS experiment could fully utilize existing spectrometers and de-  
113 tectors at JLab, upon examining all existing techniques for PV measurements it  
114 became clear that a custom electronics and DAQ were needed to control the sys-  
115 tematic uncertainties due to data collection to below 1%. In this paper we describe  
116 a scaler-based, cost effective counting DAQ which limited the pion contamination  
117 of the data sample to a negligible level of  $f \approx 10^{-3}$ . Basic information of the de-  
118 tector package and the DAQ setup will be presented first, followed by the analysis  
119 on electron detection efficiency, pion rejection and contamination, corrections due  
120 to counting deadtime, and the statistical quality of the asymmetry measurement.

## 121 **2 Detector and DAQ Overview**

122 The design goal of the DAQ is to record data up to 1 MHz with hardware-based  
123 PID and well measured and understood deadtime effects. The following detectors  
124 in the HRS [5] were used to characterize scattered particles: Two scintillator planes  
125 provided the main trigger, while a CO<sub>2</sub> gas Cherenkov detector and a double-layer  
126 segmented lead-glass detector provided particle identification information. The ver-  
127 tical drift chambers (as the tracking detector) were used during calibration runs but  
128 were turned off during production data taking because they were not expected to  
129 endure the high event rates.

130 For the gas Cherenkov and the lead-glass detector, a full recording of their out-  
131 put ADC data is not feasible at the expected high rate. Instead their signals were  
132 passed through discriminators and logic units to form preliminary electron and pion  
133 triggers. Particle identification was fulfilled by the use of discriminators for both  
134 the lead-glass and the Cherenkov detectors and proper settings of their thresholds.  
135 These preliminary triggers were then combined with the scintillator triggers to form  
136 the final electron and pion triggers, which were sent to scalars to record the event  
137 counts and offline used to form asymmetries  $A = (n_R - n_L)/(n_R + n_L)$ , where  
138  $n_{R(L)}$  is the integrated rate of the triggers normalized to the integrated beam charge  
139 for the right(*R*) and left(*L*) handed spin (helicity) states of the incident electron

140 beam. The scalers that counted triggers and the beam charge were integrated over  
141 the helicity period, which was flipped pseudo-randomly at 30 Hz per the experi-  
142 mental technique used by the HAPPEX experiments [11].

143 For the HRS the two layers of the lead-glass detector are called “preshower” and  
144 “shower” detectors, respectively. The preshower blocks in the Right HRS (the spec-  
145 trometer located to the right side of the beamline when viewed along the beam  
146 direction) has 48 blocks arranged in a  $2 \times 24$  array, with the longest dimension  
147 of the blocks aligned perpendicular to the particle trajectory. For the two blocks  
148 in each row, only the ends facing outward are read out by photo-multiplier tubes  
149 (PMTs) and the other ends of the two blocks were facing each other and not read  
150 out. Therefore the preshower detector had 48 output channels. All preshower blocks  
151 were individually wrapped to prevent light leak. The shower detector in the Right  
152 HRS had 75 blocks arranged in a  $5 \times 15$  array with the longest dimension of the  
153 blocks aligned along the trajectory of scattered particles. PMTs are attached to each  
154 block of the Right shower detector on one end only, giving 75 output channels. The  
155 preshower and the shower detectors in the Left HRS are similar to the preshower  
156 detector on the Right HRS except that for each detector there are 34 blocks arranged  
157 in a  $2 \times 17$  array.

158 Because the lead-glass detectors in the Left and Right HRS are different, design of  
159 the lead-glass-based triggers of the DAQ is also different, as shown in Fig. 1. As  
160 a compromise between the amount of electronics needed and the rate in the front  
161 end logic modules, the lead-glass blocks in both the preshower and the shower de-  
162 tectors were divided into 6 (8) groups for the Left (Right) HRS, with each group  
163 consisting 8 blocks. On the Right HRS only 60 of the 75 shower blocks were used  
164 while the 15 blocks on the edge were not read out. The reduction on the HRS ac-  
165 ceptance due to not using these side blocks is negligible. Signals from the 8 blocks  
166 in each group were added using a custom-made analog summing unit called the  
167 “SUM8 module”, then passed to discriminators. The geometry and the position of  
168 each preshower group were carefully chosen to match those of the corresponding  
169 shower group to maximize electron detection efficiency. On the Left HRS adjacent  
170 groups in both preshower and shower had overlapping blocks, while for the Right  
171 HRS only preshower blocks were overlapping. To allow overlap between adjacent  
172 groups, signals from preshower blocks on the Right HRS and from both preshower  
173 and shower blocks on the Left HRS were split into two identical copies using pas-  
174 sive splitters.

175 A schematic diagram of the DAQ electronics for the Right HRS is shown in Fig. 2.  
176 Preliminary electron and pion triggers were formed by passing shower (SS) and  
177 preshower (PS) signals and their sums, called total shower (TS) signals, through  
178 discriminators with different thresholds. For electron triggers, logical ANDs of  
179 the PS discriminator and the TS discriminator outputs were used. For pions, low  
180 threshold discriminators on the TS signal alone were sent to logical OR modules  
181 to produce preliminary triggers. Additional background rejection was provided by

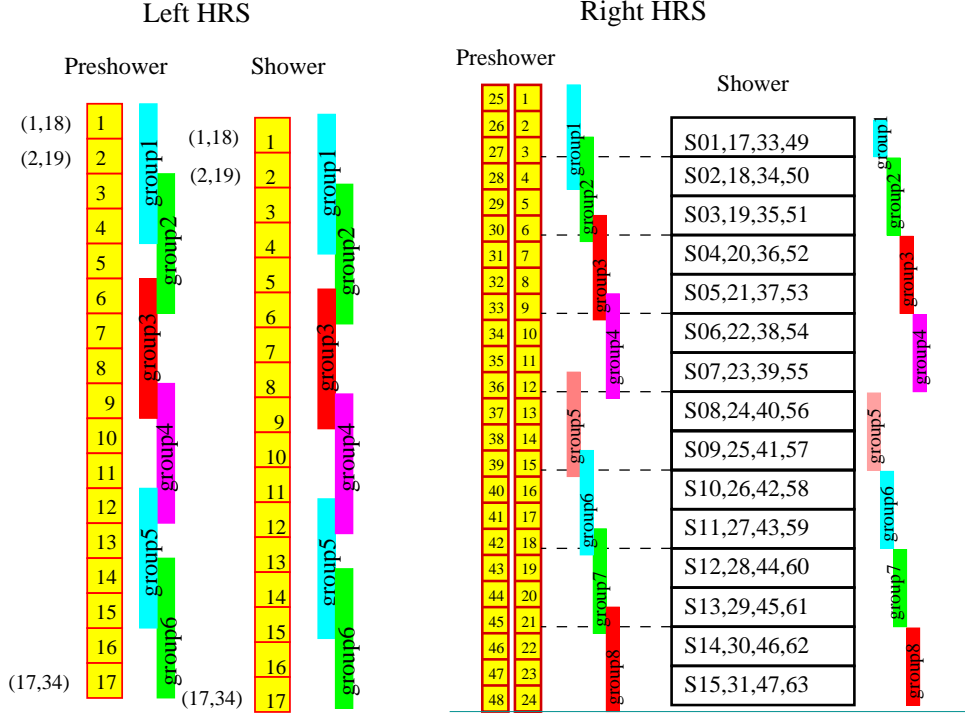


Fig. 1. [Color online] Grouping scheme (side-view) for the double-layer lead-glass detectors for the Left and the Right HRS. Scattered particles enter the detector from the left. The colored vertical bars represent the range of each group.

182 the “VETO” circuit, which combined signals from the gas Cherenkov (GC) and the  
 183 “T1” signal [5] from scintillators (SC). Each valid coincidence between GC and  
 184 T1 would produce an 150-ns wide electron VETO signal that allowed an output  
 185 to be formed by the logical AND modules from the preliminary electron triggers.  
 186 Each valid T1 signal without the GC signal would produce an 150-ns wide pion  
 187 VETO signal that allowed an output to be formed by the logical OR modules from  
 188 the preliminary pion triggers. The outputs of the logical AND and OR modules are  
 189 called group electron and pion triggers, respectively. All six (eight) group electron  
 190 or pion triggers were then ORed together to form the global electron or pion trigger  
 191 for the Left (Right) HRS. All group and the final electron and pion triggers were  
 192 counted using scalers. Because pions do not produce large enough lead-glass sig-  
 193 nals to trigger the high threshold TS discriminators for the electron triggers, pions  
 194 do not introduce extra counting deadtime for the electron triggers. However, the  
 195 150-ns width of the electron VETO signal would cause pion contamination in the  
 196 electron trigger. This effect will be presented in section 3.

197 In order to monitor the counting deadtime of the DAQ, two identical paths of elec-  
 198 tronics were constructed. The only difference between the two paths is in the PS  
 199 and the TS discriminator output widths, set at 30 ns and 100 ns for the “narrow”  
 200 and the “wide” paths, respectively. The scalers are rated for 250 MHz (4 ns dead-  
 201 time) and therefore do not add to the deadtime. In addition, the output width of all  
 202 logic modules were set to 15 ns, hence the deadtime of the DAQ for each group

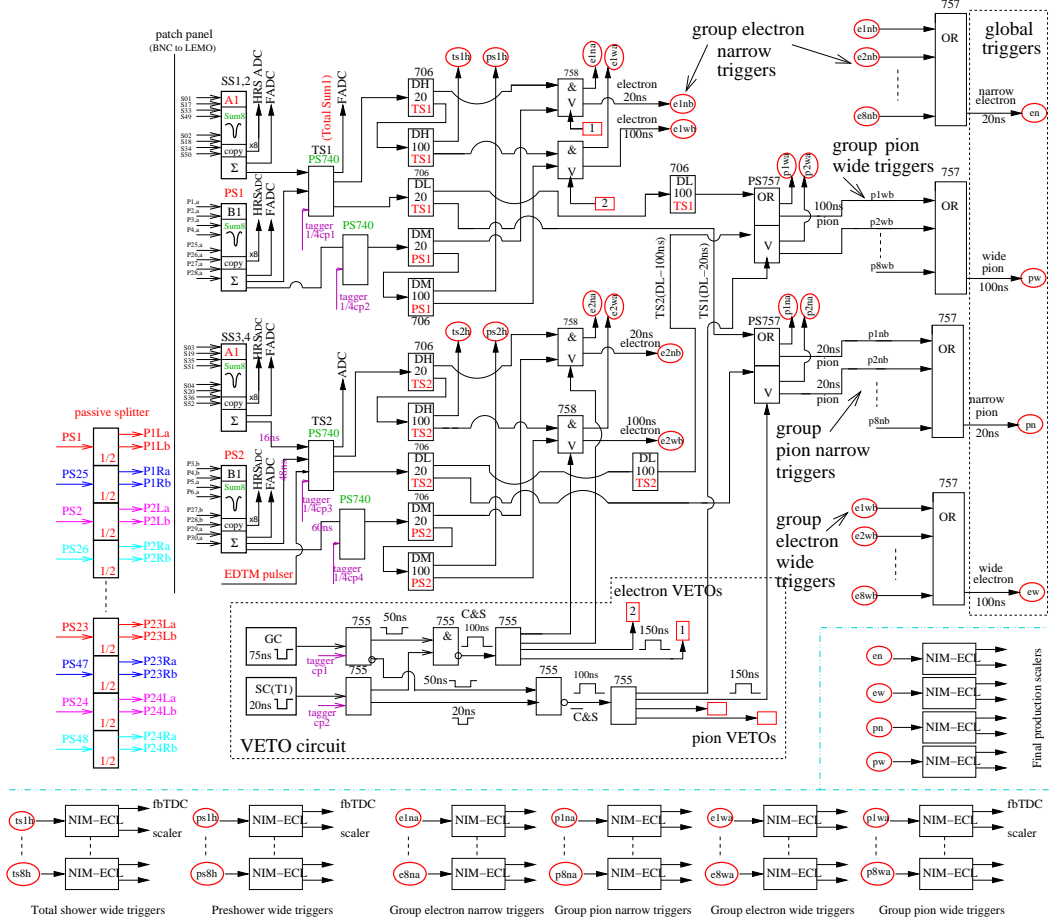


Fig. 2. [Color online] Electronics diagram for the Right HRS DAQ used by the PVDIS experiment. The Sum8's, discriminators and logic modules for two groups are shown, as well as the location of tagger signal inputs, setup of the VETO circuit using scintillator (SC) and gas Cherenkov (GC) signals, the logic units for combining triggers from all eight groups into final triggers, the counting scalars, and the monitoring fastbus TDCs. Electronics for the Left HRS are similar except for the grouping scheme.

203 is dominated by the deadtime of the discriminators. Detailed analysis of the DAQ  
 204 deadtime will be presented in section 4.

205 The SUM8 modules used for summing all lead-glass signals also served as fan-out  
 206 modules, providing exact copies of the input PMT signals. These copies were sent  
 207 to the standard HRS DAQ for calibration. During the experiment, data were col-  
 208 lected at low rates using reduced beam currents with both DAQs functioning, such  
 209 that a direct comparison of the two DAQs can be made. The vertical drift chambers  
 210 were used during these low rate DAQ studies. Outputs from all discriminators, sig-  
 211 nals from the scintillator and the gas Cherenkov, and all electron and pion group  
 212 and global triggers were sent to Fastbus TDCs (fbTDC) and were recorded in the  
 213 standard DAQ. Data from these fbTDCs were used to align amplitude spectrum  
 214 and timing of all signals. They also allowed the study of the Cherenkov and the  
 215 lead-glass detector performance for the new DAQ.

216 Full sampling of partial analog signals were done using Flash-ADCs (FADCs) at  
 217 low rates intermittently during the experiment. For one group on the Left and one  
 218 group on the Right HRS, the preshower and the shower SUM8 outputs, the inter-  
 219 mediate logical signals of the DAQ, and the output electron and pion triggers were  
 220 recorded. These FADC data provided a study of pileup effects to confirm the dead-  
 221 time simulation and to provide the input parameters for the simulation, specifically  
 222 the rise and fall times of the signals and their widths.

### 223 3 DAQ PID Performance

224 PID performance of the DAQ system was studied with calibration runs taken at low  
 225 beam currents using fbTDC signals along with ADC data of all detector signals  
 226 recorded by the standard DAQ. Events that triggered the DAQ would appear as  
 227 a timing peak in the corresponding fbTDC spectrum of the standard DAQ and a  
 228 cut on this peak can be used to select those events. Figure 3 shows the preshower  
 229 vs. shower signals for group 2 on the Left HRS. A comparison between no fbTDC  
 230 cut and with cut on the fbTDC signal of the electron wide trigger from this group  
 clearly shows the hardware PID cuts.

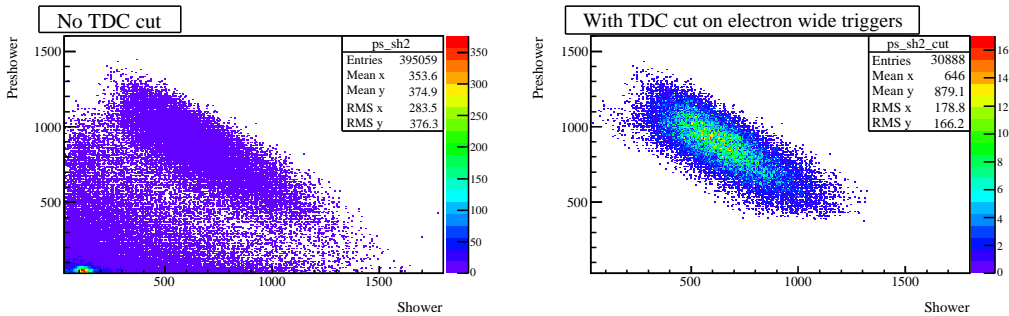


Fig. 3. [Color online] Preshower vs. Shower ADC data (sum of 8 blocks each) for group 2 on the Left HRS, without the fbTDC cut (left panel) and with cut on the group 2 electron wide trigger fbTDC signal (right panel). It clearly shows the thresholds on the preshower and the total shower signals, indicating the DAQ is selecting the correct events as electrons.

231

232 Electron efficiency and pion rejection factors of the lead-glass detector on the Left  
 233 HRS during a one-hour run are shown in Fig. 4 as functions of the location of the  
 234 hit of the particle in the preshower detector. PID performance on the Right HRS  
 235 is similar. Electron efficiency from wide groups are slightly higher than narrow  
 236 groups because there is less event loss due to timing mis-alignment when taking  
 237 the coincidence between the preshower and the total shower discriminator outputs.  
 238 Variations in the electron efficiency across the spectrometer acceptance effectively  
 239 influence the  $Q^2$  of the measurement. For this reason, low-rate calibration data  
 240 were taken daily during the experiment to monitor the DAQ PID performance and  
 241 corrections were applied to the asymmetry data.

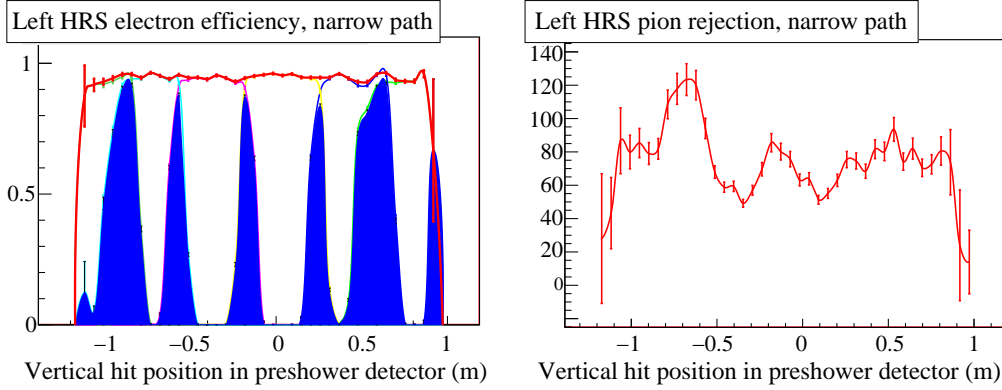


Fig. 4. [Color online] Electron detection efficiency (left) and pion rejection factor (right) vs. vertical (dispersive) hit position of the particle in the preshower detector for the narrow electron triggers in the Left HRS. A one-hour run was used in this evaluation. For electron efficiencies, the total efficiency is shown by the red curve, while blue shaded area indicates events that were recorded by two adjacent groups. The average electron efficiency achieved by the lead glass detector alone for this one-hour run is  $(94.626 \pm 0.002)\%$  and the average pion rejection factor is  $(75.3 \pm 1.1) : 1$ . The error bars are statistical only. PID performance for the wide path and the Right HRS are similar.

242 The gas Cherenkov detector signals were read out by 10 PMTs on both the Left and  
 243 the Right HRS. Signals from all 10 PMTs were summed in an analog-sum module  
 244 and sent to a discriminator. The discriminator output was sent to the DAQ (as shown  
 245 in Fig. 2) as well as fbTDCs. Figure 5 shows the Cherenkov ADC sum with and  
 246 without the fbTDC cut which clearly shows the capability of rejecting pions.

247 As described in the Introduction, pion contamination in the electron trigger would  
 248 affect the measured electron asymmetry as  $A_m = (1 - f)A_e + fA_\pi$  where  $A_m$   
 249 and  $A_e$  are the measured and the true electron asymmetries, respectively, and  $A_\pi$  is  
 250 the parity violation asymmetry of pion production. The pion contamination in the  
 251 electron trigger,  $f$ , comes from two effects: There is a small possibility that a pion  
 252 could trigger both the lead-glass and the gas Cherenkov detectors, causing a false  
 253 electron trigger output. This possibility is determined by the direct combination of  
 254 the pion rejection factors of the two detectors and is at the  $10^{-4}$  level. A larger  
 255 effect comes from the width of the electron VETO signal: Since each coincidence  
 256 between the gas Cherenkov and the scintillator signals would open the electron  
 257 counting gate (electron VETO) by 150 ns, while the DAQ deadtime of the lead-  
 258 glass detector is less than this value, pions that arrived after the DAQ deadtime but  
 259 before the closing of the electron VETO signal would cause a false electron trigger.  
 260 The sum of the two effects can be written as

$$f_{n(w)} = \frac{R_\pi \eta_\pi^{GC} \eta_\pi^{LG}}{R_e \eta_e^{GC} \eta_e^{LG}} + \frac{R_\pi \eta_\pi^{LG} \left\{ R_e \eta_e^{GC} [150 \text{ ns} - \tau_{n(w)}] \right\}}{R_e \eta_e^{GC} \eta_e^{LG}}$$

261 where  $R_e$  and  $R_\pi$  are the input electron and the pion rates, respectively;  $\eta_e^{LG(GC)}$

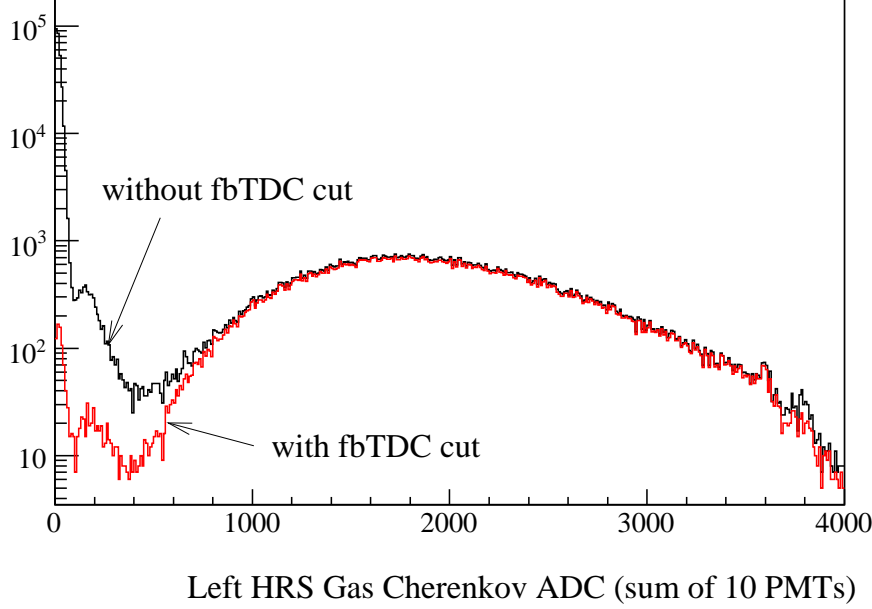


Fig. 5. [Color online] Gas Cherenkov ADC data (sum of 10 PMTs) for the Left HRS during a one-hour run, with a fbTDC cut on the Cherenkov discriminator output (red) and without (black). The discriminator clearly selected electrons while rejecting pions.

262 is the electron detection efficiency of the lead-glass (gas Cherenkov) detectors, and  
 263  $\eta_{\pi}^{LG(GC)}$  is the pion detection efficiency, i.e., the inverse of the rejection factor, of  
 264 the lead-glass (gas Cherenkov) detector. The DAQ group deadtime of the lead-glass  
 265 detector for the narrow (wide) path,  $\tau_{n(w)}$ , is approximately 60 ns (100-110 ns) and  
 266 the analysis obtaining these results will be presented in the next section. The term  
 267  $R_e \eta_e^{GC} [150 \text{ ns} - \tau_{n(w)}]$  gives the probability for a pion to arrive within a valid  
 268 electron VETO signal.

269 The electron detection efficiency and pion rejection factor averaged throughout the  
 270 experiment are shown in Table 1 for different kinematics and for the Left and the  
 271 Right HRS separately. Also shown are the  $\pi/e$  rate ratio obtained from the data  
 272 and the resulting pion contamination  $f$  evaluated separately for the narrow and the  
 273 wide paths.

274 As shown in table 1, the overall pion contamination was at the order of  $2 \times 10^{-3}$   
 275 or lower. Because pions are produced from nucleon resonance decays, the parity  
 276 violation asymmetry of pion production is expected to be no larger than that of  
 277 scattered electrons with the same momentum. This was confirmed by asymmetries  
 278 formed from pion triggers during this experiment. The uncertainty in the electron  
 279 asymmetry due to pion contamination is therefore at the order of  $2 \times 10^{-3}$  and is  
 280 negligible compared to the 3 – 4% statistical uncertainty.

Table 1

Average electron detection efficiency and pion rejection factor achieved through the lead glass (LG) and the gas Cherenkov (GC) detectors, respectively, and the combined performance. The error bars of the efficiencies and the rejection factors are statistical only.

| Electron detection efficiency $\eta_e$            |                               |                               |                       |
|---|-------------------------------|-------------------------------|-----------------------|
|   | $Q^2 = 1.1 \text{ (GeV}/c)^2$ | $Q^2 = 1.9 \text{ (GeV}/c)^2$ |                       |
| HRS   | Left                          | Left                          | Right                 |
| LG  | $(91.93 \pm 0.04)\%$          | $(94.50 \pm 0.06)\%$          | $(94.36 \pm 0.04)\%$  |
| GC  | $(99.14 \pm 0.02)\%$          | $(99.03 \pm 0.03)\%$          | $(98.19 \pm 0.06)\%$  |
| combined  | $(91.14 \pm 0.04)\%$          | $(93.58 \pm 0.06)\%$          | $(92.65 \pm 0.07)\%$  |
| Pion rejection $1/\eta_\pi$ and contamination $f$ |                               |                               |                       |
|   | $Q^2 = 1.1(\text{GeV}/c)^2$   | $Q^2 = 1.9(\text{GeV}/c)^2$   |                       |
| HRS   | Left                          | Left                          | Right                 |
| LG  | $(101.5 \pm 1.6) : 1$         | $(78.9 \pm 0.9) : 1$          | $(72.7 \pm 0.3) : 1$  |
| GC  | $(158.6 \pm 3.5) : 1$         | $(301.2 \pm 5.2) : 1$         | $(414.3 \pm 6.2) : 1$ |
| $R_\pi/R_e$                                       | 0.7                           | 3.5                           | 3.5                   |
| $f_n$   | $1.61 \times 10^{-3}$         | $2.22 \times 10^{-3}$         | $1.95 \times 10^{-3}$ |
| $f_w$   | $1.05 \times 10^{-3}$         | $1.86 \times 10^{-3}$         | $1.54 \times 10^{-3}$ |

## 281 4 DAQ Deadtime

282 Deadtime is the amount of time after an event during which the system is unable  
 283 to record another event. Identifying the exact value of the deadtime is always a  
 284 challenge in counting experiments. By having a narrow and a wide path, we can  
 285 observe the trend in the deadtime – the wider path should have higher deadtime. By  
 286 matching the observed trend with our simulation we can benchmark and confirm  
 287 the result of our deadtime simulation. In addition, dividing lead-glass blocks into  
 288 groups greatly reduces the deadtime loss in each group compared to summing all  
 289 blocks together and forming only one final trigger.

290 To illustrate the importance of the deadtime, consider its effect on the asymmetry  $A$ .  
 291 For a simple system with only one contribution to the deadtime loss  $\delta$ , the observed  
 292 asymmetry  $A_O$  is related to the true asymmetry  $A$  according to  $A_O = (1 - \delta)A$ .  
 293 In this experiment  $\delta$  was expected to be on the order of (1-2)%. Since the statistical  
 294 accuracy on the asymmetry is (3-4)%, it was desired to know  $\delta$  with a (10-20)%  
 295 relative accuracy so that it would become a negligible systematic error. The DAQ  
 296 used in this experiment, however, was more complex and had three contributions  
 297 to the deadtime as listed below:

- 298 (1) The “group” deadtime: deadtime due to discriminators and logical AND mod-  
 299 ules used to form group triggers;
- 300 (2) The “veto” deadtime: deadtime from the VETO circuit that used scintillators  
 301 and gas Cherenkov signals to form the “gate” signals, which controlled the  
 302 AND (OR) module of each group to form group electron (pion) triggers.
- 303 (3) The “OR” deadtime: deadtime due to the logical OR module used to combine  
 304 all group triggers into final global triggers.

305 The total deadtime is a combination of all three. In order to evaluate the DAQ  
 306 deadtime, a full-scale simulation was developed as follows: The analog signals for  
 307 preshower, shower, scintillator and gas Cherenkov as recorded by ADCs from low-  
 308 current runs were fed to the simulation as inputs. For the preshower and shower  
 309 SUM8 outputs, FADC data were used to determine the rise and the fall time of  
 310 the signal. The simulation took into account all electronics and delay cables of the  
 311 DAQ and calculated digital outputs from all discriminators, AND, and OR modules,  
 312 providing results on the fractional loss due to deadtime for all group and global  
 313 triggers w.r.t. the input signal.

#### 314 4.1 Group Deadtime Measurement

315 In order to study the group deadtime, a high rate pulser signal (“tagger”) was mixed  
 316 with the Cherenkov and all preshower and total shower signals using analog sum-  
 317 ming modules, see Figs. 2 and 6. In the absence of all detector signals, a tagger  
 318 pulse produces without loss an electron trigger output, and a “tagger-trigger coin-  
 319 cidence” pulse between this output and the “delayed tagger” – the tagger itself with  
 320 an appropriate delay to account for the DAQ response time. When high-rate detec-  
 321 tor signals are present, however, some of the tagger pulses would not be able to  
 322 trigger the DAQ due to deadtime. The deadtime loss in the electron trigger output  
 323 w.r.t. the tagger input has two components:

- 324 (1) The count loss  $R_o/R_i$ : when a detector PMT signal precedes the tagger signal  
 325 by a time interval  $\delta t$  shorter than the DAQ deadtime but longer than  $w + t_1$ , the  
 326 tagger signal is lost and no coincidence output is formed. Here  $w$  is the width  
 327 of the electron trigger output and  $t_1$  is the time interval the delayed tagger  
 328 precedes the tagger’s own trigger output, see Fig. 6. During the experiment  $w$   
 329 was set to 15 ns for all groups,  $t_1$  was measured at the end of the experiment  
 330 and was found to be between 20 and 40 ns for all narrow and wide groups of  
 331 the two HRSs.
- 332 (2) The pileup fraction  $p$ : when a PMT signal precedes the tagger signal by a time  
 333 interval  $\delta t$  shorter than  $w + t_1$ , there would be coincidence output between the  
 334 delayed tagger and the electron output triggered by the detector PMT signal.  
 335 If furthermore  $\delta t$  is less than the DAQ deadtime (which is possible for this  
 336 experiment since the deadtime is expected to be as long as 100 ns for the wide

337 path), the tagger itself is lost due to deadtime and the tagger-trigger coinci-  
 338 dence is a false count and should be subtracted. In the case if  $\delta t$  is shorter than  
 339  $w + t_1$  but longer than the DAQ deadtime (not possible for this experiment  
 340 but could happen in general), the tagger itself also triggers a tagger-trigger  
 341 coincidence but in this case, there are two tagger-trigger coincidence events,  
 342 both are recorded by the fbTDC if working in the multi-hit mode, and one is  
 343 a false count and should be subtracted.

344 The pileup effect can be measured using the delay between the tagger-  
 345 trigger coincidence output and the input tagger. This is illustrated in Fig. 6  
 346 and the pileup effect contributes to both  $I_1$  and  $I_2$  regions of the fbTDC spec-  
 347 trum. Fractions of  $I_1$  and  $I_2$  relative to  $I_0$  are expected to be  $I_1/I_0 = Rt_1$  and  
 348  $I_2/I_0 = Rw$ , respectively, where  $R$  is the PMT signal rate. The pileup effect  
 349 was measured using fbTDC spectrum for electron narrow and wide triggers  
 350 for all groups. Data for  $I_{1,2}$  extracted from fbTDC agree very well with the  
 351 expected values.

The relative loss of tagger events due to DAQ deadtime is evaluated as

$$D = 1 - (1 - p)(R_o/R_i), \quad (3)$$

352 where  $R_i$  is the input tagger rate,  $R_o$  is the output tagger-trigger coincidence rate,  
 353 and  $p = (I_1 + I_2)/I_0$  is a correction factor for pileup effects as defined in Fig. 6.  
 354 Results for the deadtime loss  $D$  are shown in Figs. 7 and 8, for group 4 on the left  
 355 HRS and group 4 on the right HRS, respectively, and are compared with simulation.  
 356 Different beam currents between 20 and 100  $\mu\text{A}$  were used in this dedicated dead-  
 357 time measurement. In order to reduce the statistical fluctuation caused by limited  
 358 number of trials in the simulation within a realistic computing time, simulations  
 359 were done at higher rates than the actual measurement.

360 The slope of the tagger loss vs. event rate, as shown in Figs. 7 and 8, gives the value  
 361 of group deadtime in seconds. One can see that the deadtime for the wide path is  
 362 approximately 100 ns as expected. The deadtime for the narrow path, on the other  
 363 hand, is dominated by the input PMT signal width (typically 60-80 ns) instead of  
 364 the 30-ns discriminator width. The simulated deadtime agree very well with data  
 365 for both HRSs and for both wide and narrow paths.

## 366 4.2 Total Deadtime Evaluation

367 Although the deadtime loss of each group was measured using tagger signals, the  
 368 dominating term in the total deadtime is from the veto electronics because the trig-  
 369 ger rate from scintillators and the gas Cherenkov is much higher than the individual  
 370 lead-glass group rates. The difference in total loss between narrow and wide path  
 371 is thus smaller than that in their group deadtimes. Simulation for the veto dead-  
 372 time was compared with FADC data and the agreement was found to be at 20%

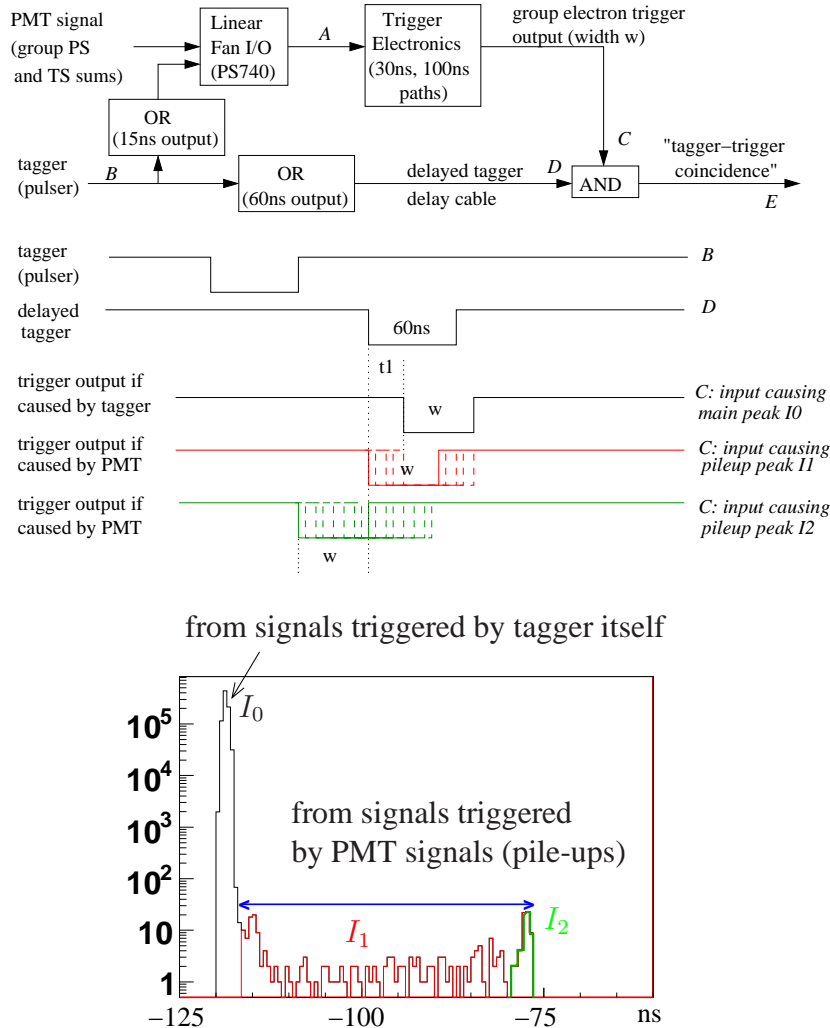


Fig. 6. [Color online] Top: schematic diagram for the tagger setup and signal timing sequence. The two logical OR units immediately following the tagger input “B” serve as width adjusters. Bottom: fbTDC spectrum for the relative timing between tagger-trigger coincidence and the input tagger, in 0.5-ns bins. The fbTDC module worked in a common stop and the multi-hit mode. Two different scenarios are shown: 1) Main peak  $I_0$ : when there is no PMT signal preceding the tagger, the tagger triggers the DAQ and forms a tagger-trigger coincidence. 2) Pileup events  $I_1$  and  $I_2$ : when there is a PMT signal preceding the tagger by a time interval shorter than  $w + t_1$ , the PMT signal triggers the DAQ and forms a tagger-trigger coincidence signal with the delayed tagger.

373 level or better. After subtracting group and veto deadtimes from the total simulated  
 374 deadtime, the remaining is attributed to the logical OR module. There is no direct  
 375 measurement of the logical OR deadtime, but the effect of the logical OR module  
 376 is quite straightforward and can be calculated analytically. The difference between  
 377 the simulation and the analytic results was used to estimate the uncertainty of the  
 378 OR deadtime.

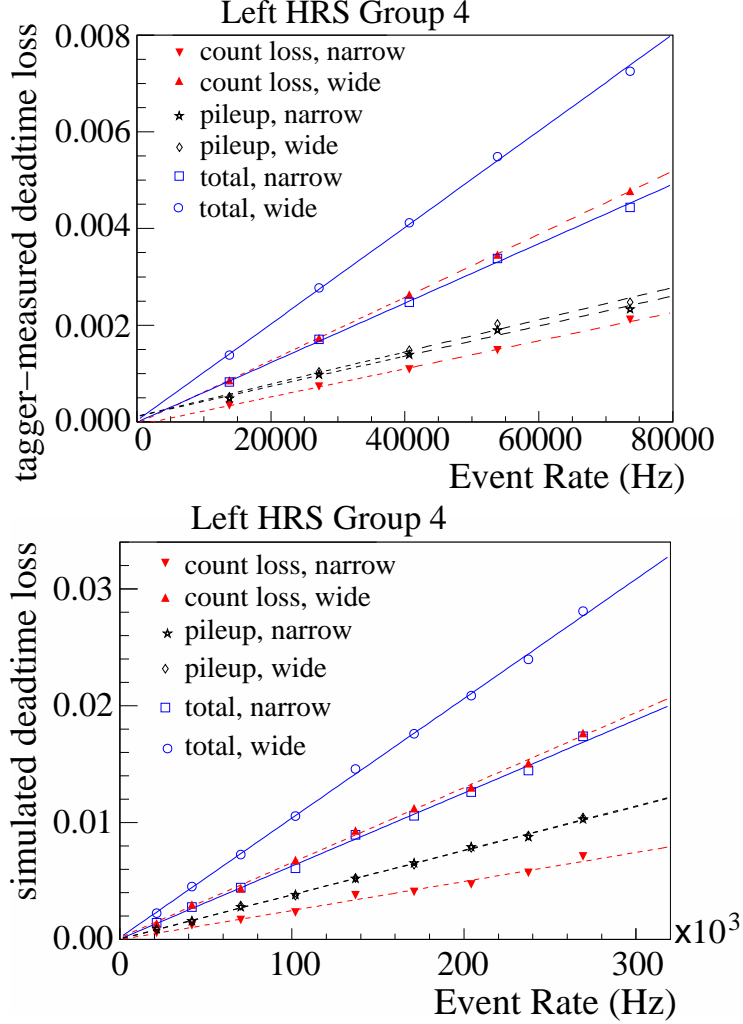


Fig. 7. [Color online] Deadtime loss in percent vs. event rate from the tagger method for group 4 on the Left HRS. Top: actual deadtime loss from tagger measurements; Bottom: simulated deadtime loss of the tagger. The tagger fractional count loss  $1 - R_o/R_i$  (red) and the pileup correction  $p$  (black) are combined to form the total group deadtime  $D$  (blue). These data were taken (or simulated) at a  $Q^2$  of 1.1 (GeV/c)<sup>2</sup>. To minimize the statistical uncertainty while keeping the computing time reasonable, the simulation used higher event rates than the tagger measurement. The total group deadtime can be determined from the linear fit slope coefficients: tagger data narrow  $p_1 = (61.5 \pm 0.2) \times 10^{-9}$  s, wide  $p_1 = (99.9 \pm 0.3) \times 10^{-9}$  s, simulation narrow  $p_1 = (62.5 \pm 1.4) \times 10^{-9}$  s, wide  $p_1 = (102 \pm 1.3) \times 10^{-9}$  s. Group 4 is from the central blocks of the lead-glass detector and has the highest rate among all groups.

379 The simulated deadtime loss of the global electron triggers and its decomposition  
 380 into group, veto, and OR are shown in Table 2. The deadtime loss is also shown  
 381 in Fig. 9 as a function of the total event rate. The deadtime corrections to the final  
 382 asymmetry results for the narrow path triggers are  $(1.45 \pm 0.13)\%$  and  $(0.89 \pm$   
 383  $0.20)\%$ , and for the wide path triggers are  $(1.64 \pm 0.16)\%$  and  $(0.93 \pm 0.22)\%$ , for  
 384  $Q^2 = 1.1$  and  $1.9$  (GeV/c)<sup>2</sup>, respectively. These provide a direct correction to the

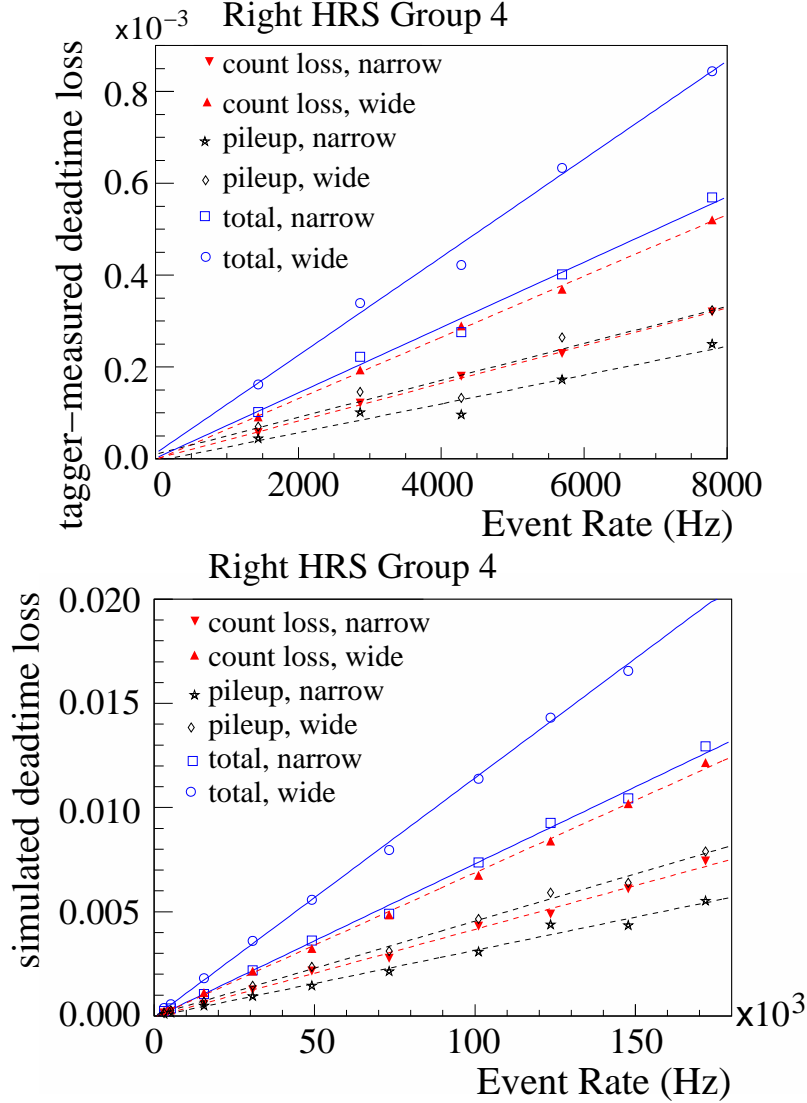


Fig. 8. [Color online] Deadtime loss in percent vs. group event rate from the tagger method for group 4 on the Right HRS. Top: tagger data; Bottom: simulation. These data were taken (or simulated) at a  $Q^2$  of 1.9 (GeV/c) $^2$ . The total group deadtime can be determined from the linear fit slope coefficient  $p_1$ : tagger data narrow  $p_1 = (71.1 \pm 0.9) \times 10^{-9}$  s, wide  $p_1 = (107 \pm 1.2) \times 10^{-9}$  s, simulation narrow  $p_1 = (73.9 \pm 1.5) \times 10^{-9}$  s, wide  $p_1 = (115 \pm 1.5) \times 10^{-9}$  s. Group 4 is from the central blocks of the lead-glass detector and has the highest rate among all groups. See Fig. 7 caption for details.

385 measured asymmetry and the uncertainties are small compared to other dominant  
 386 systematic uncertainties such as the beam polarization measurement.

Table 2

Simulated DAQ deadtime loss in percent and the fractional contributions from group, veto, and OR deadtimes. The fractional deadtime from OR is calculated as one minus those from group and veto, and its uncertainty is estimated from the difference between simulation and the analytical results. The uncertainty of the total deadtime is the uncertainties from group, veto and OR added in quadrature.

| $Q^2$<br>(GeV/c) <sup>2</sup> | Path   | fractional contribution |                    |                    | Total deadtime<br>loss at 100 $\mu$ A |
|-------------------------------|--------|-------------------------|--------------------|--------------------|---------------------------------------|
|                               |        | Group                   | Veto               | OR                 |                                       |
| 1.1                           | narrow | (20.6 $\pm$ 2.1)%       | (51.3 $\pm$ 1.9)%  | (28.1 $\pm$ 8.6)%  | (1.45 $\pm$ 0.13)%                    |
|                               | wide   | (29.5 $\pm$ 2.4)%       | (45.3 $\pm$ 1.7)%  | (25.3 $\pm$ 9.0)%  | (1.64 $\pm$ 0.16)%                    |
| 1.9                           | narrow | (2.9 $\pm$ 0.2)%        | (80.6 $\pm$ 18.5)% | (16.5 $\pm$ 12.3)% | (0.89 $\pm$ 0.20)%                    |
|                               | wide   | (4.3 $\pm$ 0.4)%        | (76.6 $\pm$ 17.5)% | (19.1 $\pm$ 15.1)% | (0.93 $\pm$ 0.22)%                    |

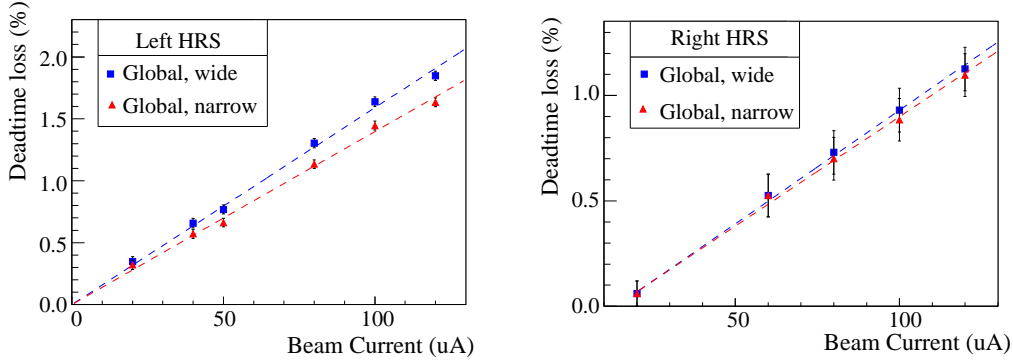


Fig. 9. [Color online] Simulated deadtime loss of the global electron trigger for the Left (left) and the Right (right) HRS. The error bars shown are due to statistical uncertainty of the simulation. See Table 2 for final uncertainty evaluation.

### 387 4.3 Asymmetry Measurement

388 The physics asymmetries sought for in this experiment were expected to be 91 and  
 389 160 ppm, for  $Q^2 = 1.1$  and  $1.9$  (GeV/c)<sup>2</sup>, respectively. The measured asymmetries  
 390 were about 90% of these values due to beam polarization. To understand the sys-  
 391 tematics of the asymmetry measurement, a half-wave plate (HWP) was inserted in  
 392 the beamline to flip the laser helicity in the polarized source during half of the data  
 393 taking period. The measured asymmetries flipped sign for each beam HWP change  
 394 and the magnitude of the asymmetry remained consistent within statistical error  
 395 bars.

396 The asymmetries can be formed from event counts of each beam helicity pair, with  
 397 33-ms of helicity right and 33-ms of helicity left beam, normalized by the beam  
 398 charge. Figure 10 shows the pull distribution of these pair-wise asymmetries with  
 399 the “pull” defined as

$$p_i \equiv (A_i - \langle A \rangle) / \delta A_i, \quad (4)$$

400 where  $A_i$  is the asymmetry extracted from the  $i$ -th beam helicity pair with the HWP  
 401 states already corrected and  $\delta A_i = 1/\sqrt{N_i^R + N_i^L}$  its statistical uncertainty with  
 402  $N_i^{R(L)}$  the event count from the right (left) helicity pulse of the pair, and  $\langle A \rangle$  is the  
 403 asymmetry averaged over all beam pairs. One can see that the asymmetry spectrum  
 404 agrees to five orders of magnitude with the Gaussian distribution, as expected from  
 405 purely statistical fluctuations.

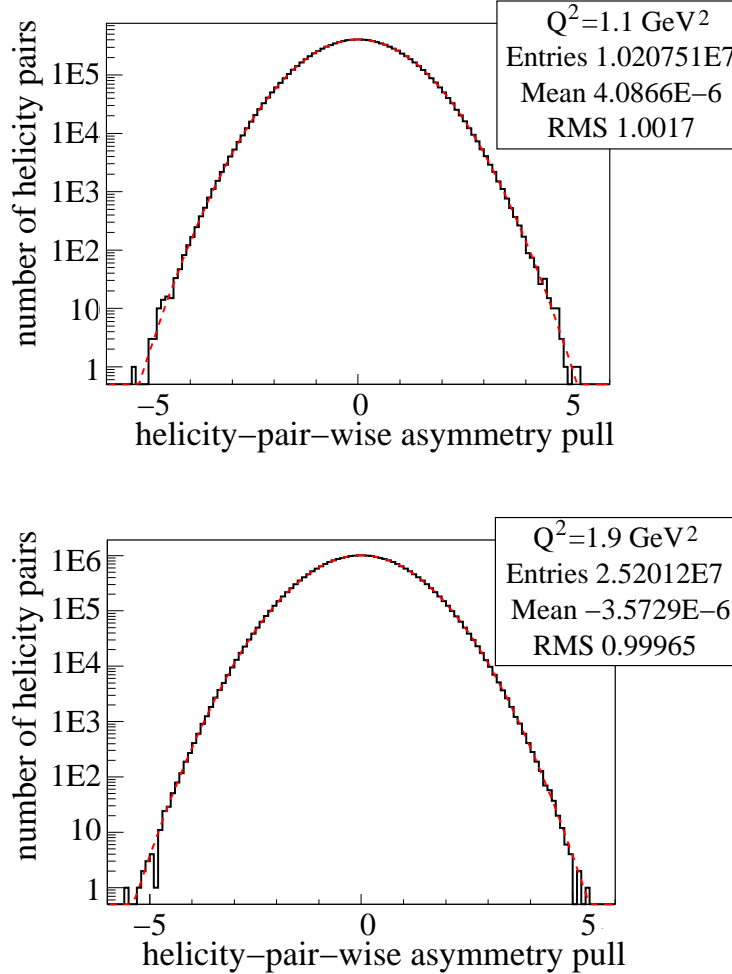


Fig. 10. [Color online] Pull distribution [Eq.(4)] for the global electron narrow trigger for  $Q^2 = 1.1$  (top) and  $Q^2 = 1.9$  (GeV/c)<sup>2</sup> (bottom).

## 406 5 Summary

407 A scaler-based counting DAQ with hardware-based particle identification was suc-  
 408 cessfully implemented in the 6 GeV PVDIS experiment at Jefferson Lab. Asymme-  
 409 tries measured by the DAQ follow Gaussian distributions as expected from purely

410 statistical measurements. Particle identification performance of the DAQ were mea-  
411 sured and corrections were applied to the data on a day-to-day basis. The overall  
412 pion contamination in the electron sample was controlled to approximately  $2 \times 10^{-3}$   
413 or lower, with an electron efficiency above 91% throughout the experiment. The  
414 DAQ deadtime was evaluated from a full-scale timing simulation and contributes  
415 an approximately 0.2% uncertainty to the final asymmetry results. The systematic  
416 uncertainties from the pion contamination and the counting deadtime are therefore  
417 both negligible compared to the (3 – 4)% statistical uncertainty and other leading  
418 systematic uncertainties. Results presented here demonstrate that accurate asymme-  
419 try measurements can be performed with even higher event rates or backgrounds  
420 with this type of scaler-based DAQ.

## 421 Acknowledgments

422 This work is supported in part by the Jeffress Memorial Trust under Award No.  
423 J-836, the U.S. National Science Foundation under Award No. 0653347, and the  
424 U.S. Department of Energy under Award No. DE-SC0003885. **Notice:** Authored  
425 by Jefferson Science Associates, LLC under U.S. DOE Contract No. DE-AC05-  
426 06OR23177. The U.S. Government retains a non-exclusive, paid-up, irrevocable,  
427 world-wide license to publish or reproduce this manuscript for U.S. Government  
428 purposes.

## 429 References

- 430 [1] JLab experiment E08-011 (previously E05-007), R. Michaels, P.E. Reimer and X.-C.  
431 Zheng, spokespersons.
- 432 [2] R. Subedi *et al.*, AIP proceedings of the 18<sup>th</sup> International Spin Physics Symposium  
433 (2009) 245.
- 434 [3] A publication about the E08-011 physics asymmetries is in preparation.
- 435 [4] K. Nakamura *et al.* [Particle Data Group], J. Phys. **G37**, 075021 (2010).
- 436 [5] J. Alcorn *et al.*, Nucl. Instrum. Meth. **A522** (2004) 294.
- 437 [6] R. Hasty *et al.* [SAMPLE Collaboration], Science **290**, 2117 (2000).
- 438 [7] K. A. Aniol *et al.* [HAPPEX Collaboration], Phys. Rev. C **69**, 065501 (2004).
- 439 [8] A. Acha *et al.* [HAPPEX Collaboration], Phys. Rev. Lett. **98**, 032301 (2007).
- 440 [9] K. A. Aniol *et al.* [HAPPEX Collaboration], Phys. Rev. Lett. **96**, 022003 (2006).
- 441 [10] K. A. Aniol *et al.* [HAPPEX Collaboration], Phys. Lett. B **635**, 275 (2006).

- 442 [11] Z. Ahmed *et al.* [HAPPEX Collaboration], Phys. Rev. Lett. **108**, 102001 (2012).
- 443 [12] S. Abrahamyan, Z. Ahmed, H. Albatineh, K. Aniol, D. S. Armstrong, W. Armstrong,  
444 T. Averett and B. Babineau *et al.*, Phys. Rev. Lett. **108**, 112502 (2012).
- 445 [13] C.Y. Prescott *et al.*, Phys. Lett. **B77** (1978) 347.
- 446 [14] C.Y. Prescott *et al.*, Phys. Lett. **B84** (1979) 524.
- 447 [15] F. E. Maas *et al.* [A4 Collaboration],  $Q^{*2} = 0.230-(\text{GeV}/c)^{*2}$ ,” Phys. Rev. Lett. **93**,  
448 022002 (2004).
- 449 [16] F. E. Maas, K. Aulenbacher, S. Baunack, L. Capozza, J. Diefenbach, B. Glaser,  
450 T. Hammel and D. von Harrach *et al.*,  $Q^{*2} = 0.108 (\text{GeV}/c)^{*2}$ ,” Phys. Rev. Lett.  
451 **94**, 152001 (2005).
- 452 [17] S. Baunack, K. Aulenbacher, D. Balaguer Rios, L. Capozza, J. Diefenbach, B. Glaser,  
453 D. von Harrach and Y. Imai *et al.*, Phys. Rev. Lett. **102**, 151803 (2009).
- 454 [18] D. H. Beck, Phys. Rev. D **39**, 3248 (1989).
- 455 [19] D. S. Armstrong *et al.* [G0 Collaboration], Phys. Rev. Lett. **95**, 092001 (2005).
- 456 [20] D. Androic *et al.* [G0 Collaboration], Phys. Rev. Lett. **104**, 012001 (2010).
- 457 [21] D. Marchand, J. Arvieux, G. Batigne, L. Bimbot, A. S. Biselli, J. Bouvier, H. Breuer  
458 and R. Clark *et al.* Nucl. Instrum. Meth. A **586**, 251 (2008).
- 459 [22] D. Androic *et al.* [G0 Collaboration], Nucl. Instrum. Meth. A **646**, 59 (2011).